Supplementary Information

Engineering electron distribution of Cu_2O/FeO_x@CNFs p-n heterojunction nanozyme: boosting the Fenton reaction efficiency

Shiwen Zhao[a, b], Lintao Yang[a, b], Jinggao Wu[c], Shipeng Qi[a, b], Yaojie Liu[a, b], Honglei Tian[a], Jianke Li[a, b*], Yuhuan Zhang[a, b*]

*

[a] *College of Food Engineering and Nutritional Science, Shaanxi Normal University, Xi'an, 710119, China*

[b] *University Key Laboratory of Food Processing Byproducts for Advanced Development and High Value Utilization, Xi'an, 710119, China*

[c] *School of Chemistry and Materials Engineering, Huaihua University, Hunan, 418000, China*

* Corresponding authors at: College of Food Engineering and Nutritional Science, Shaanxi Normal University, Xi'an 710119, China. E-mail: jiankel@snnu.edu.cn (J. Li), yh5zhang@snnu.edu.cn (Y. Zhang).

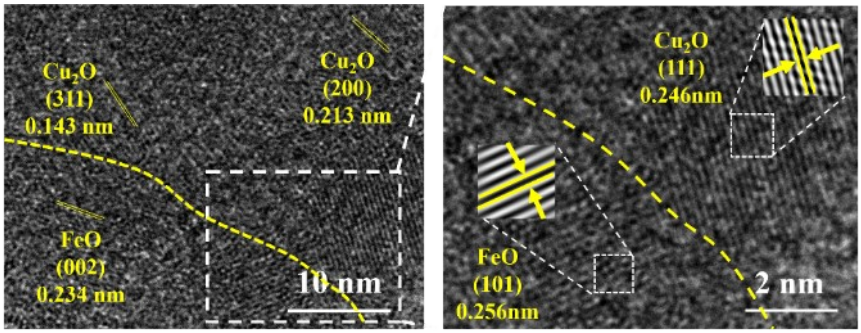

Figure S1. HRTEM and enlarged HRTEM of Cu_2O/FeO_x@CNFs.

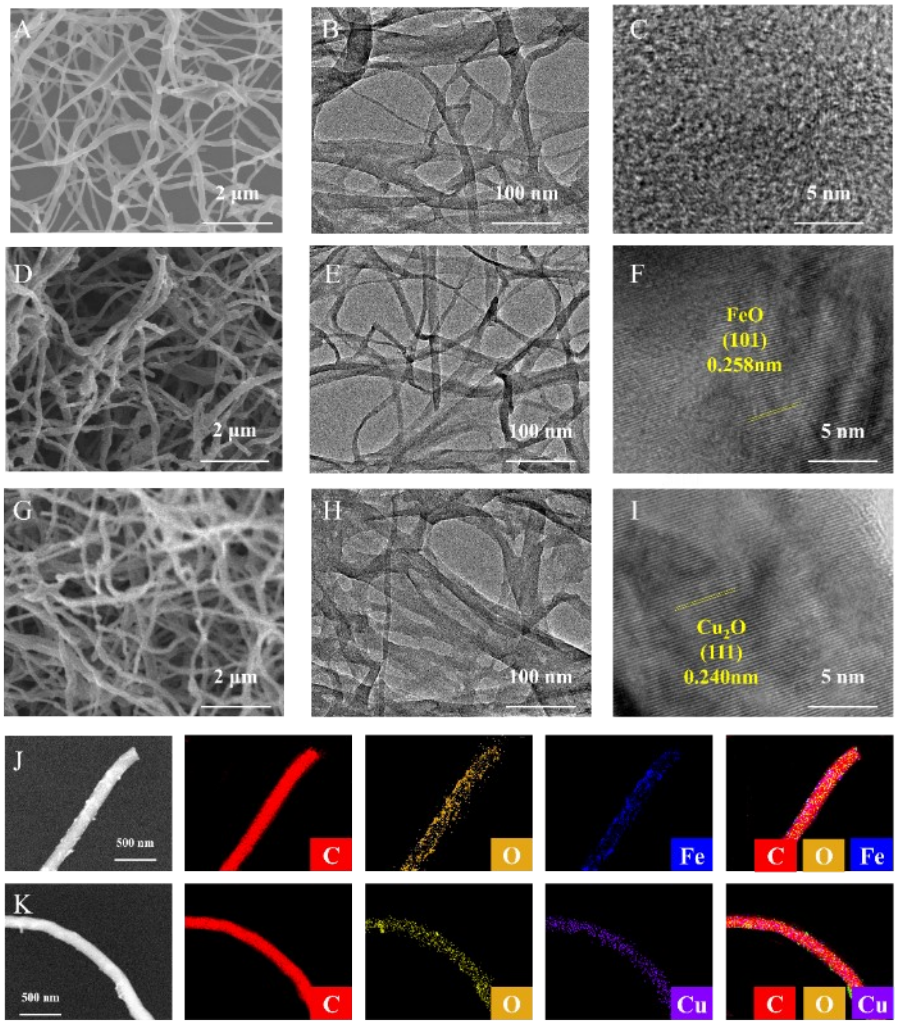

Figure S2. A) SEM image, B) TEM image and C) HRTEM of CNFs. D) SEM image, E) TEM image and F) HRTEM of FeO_x@CNFs. G) SEM image, H) TEM image and I) HRTEM of Cu_2O@CNFs. HADDF-STEM and corresponding elemental mapping images of J) FeO_x@CNFs and K) Cu_2O @CNFs.

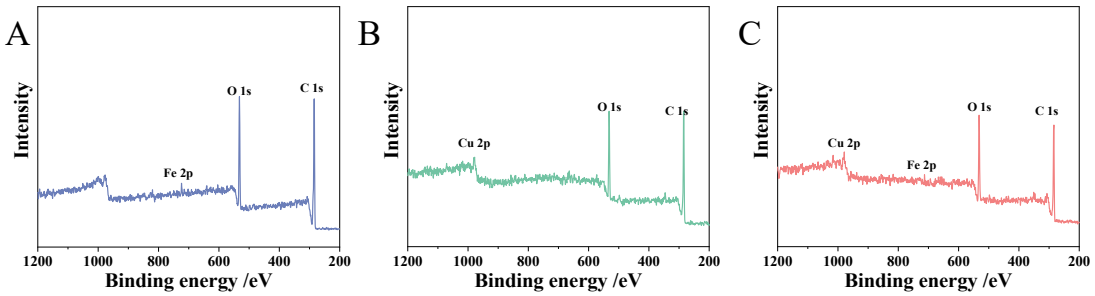

Figure S3. Full XPS survey spectra for A) FeO_x@CNFs, B) Cu_2O@CNFs and C) Cu_2O/FeO_x@CNFs.

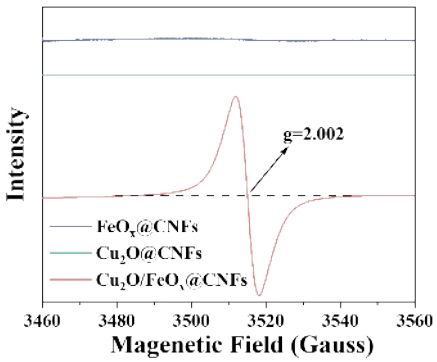

Figure S4. EPR spectra of Ov.

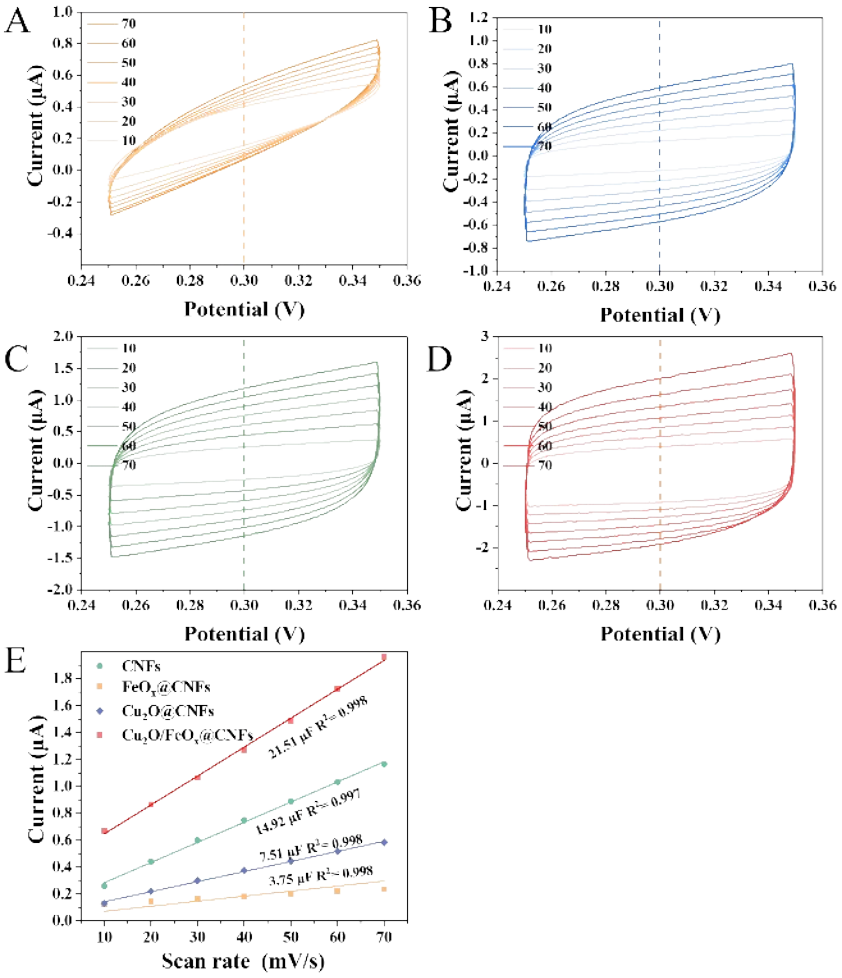

Figure S5. CV curves of A) CNFs, B) FeO_x@CNFs, C) Cu_2O@CNFs and D) Cu_2O/FeO_x@CNFs at different scan rates and E) C_{dl} of different materials.

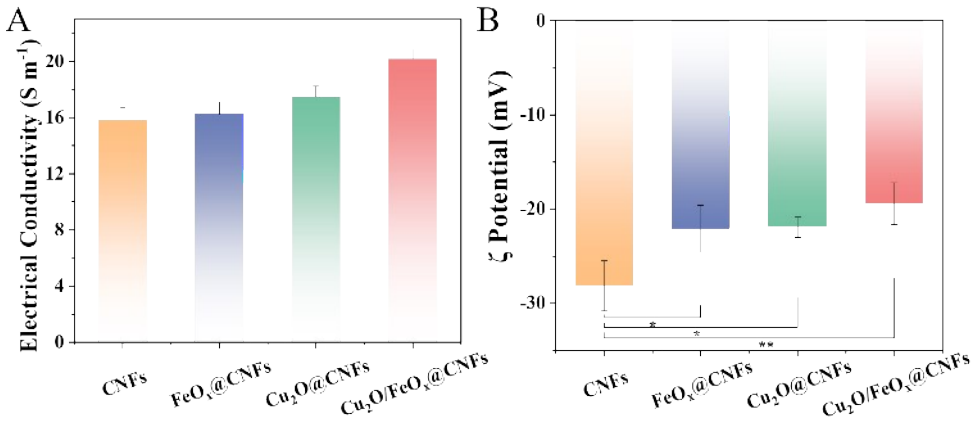

Figure S6. A) Conductivity and B) Zeta potential of different materials.

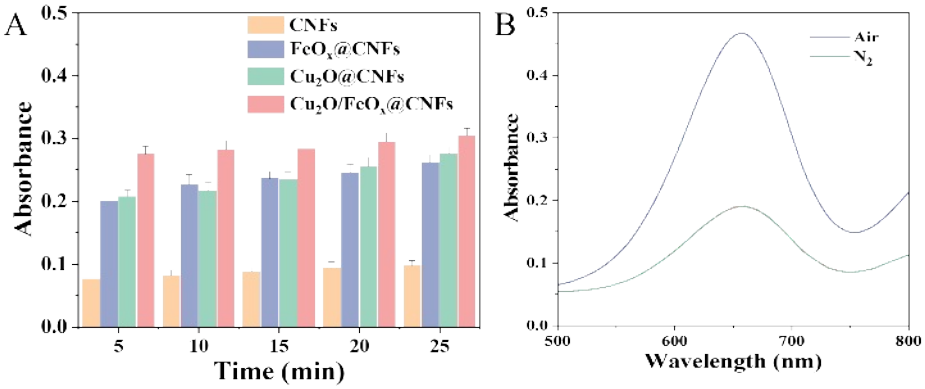

Figure S7. A) Absorbance at 652 nm of TMB reaction system corresponding to different materials at different times. B) The UV-vis spectra of TMB reaction system corresponding to Cu_2O/FeO_x@CNFs under different conditions.

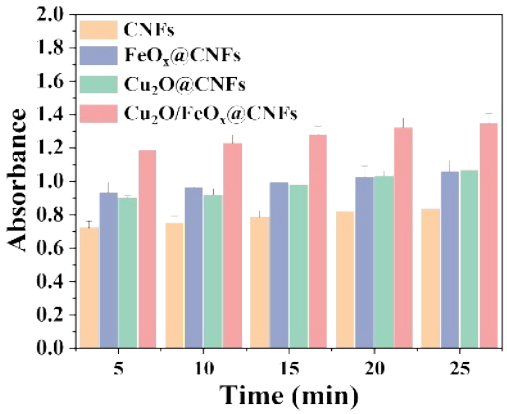

Figure S8. Absorbance at 652 nm of TMB + H_2O_2 reaction system corresponding to different materials at different times.

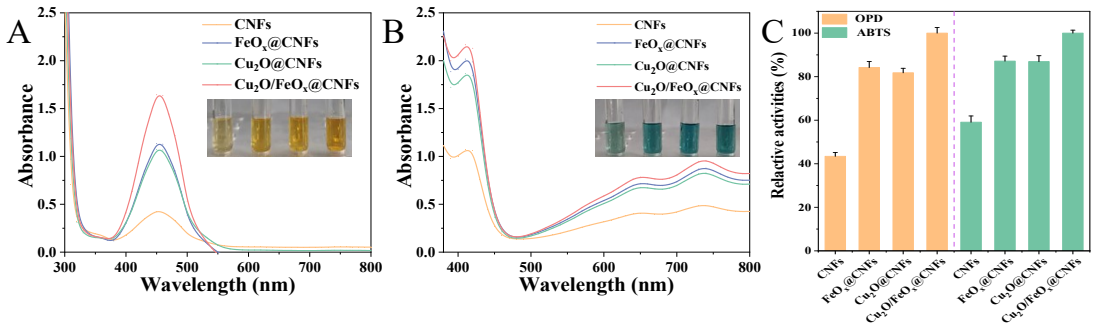

Figure S9. UV-vis spectra of A) OPD + H_2O_2 and B) ABTS + H_2O_2 mixed with different materials. Inset: color changes of different reaction systems, from left to right: CNFs, FeO_x@CNFs Cu_2O@CNFs, Cu_2O/FeO_x@CNF. C) The relative activity of different materials.

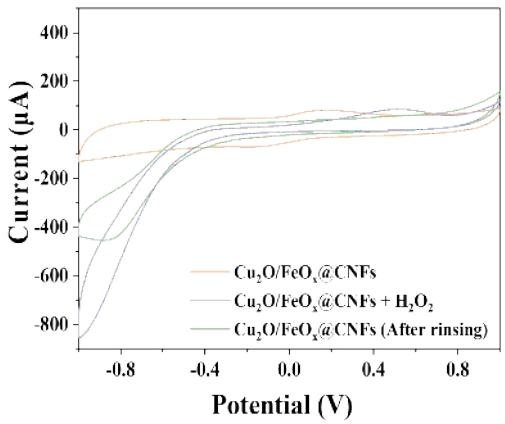

Figure S10. Typical CV curves of the Cu_2O/FeO_x@CNFs-modified glassy carbon electrode in 5 mM H_2O_2 (pink line) and after rinsing the electrode three times with water (green line).

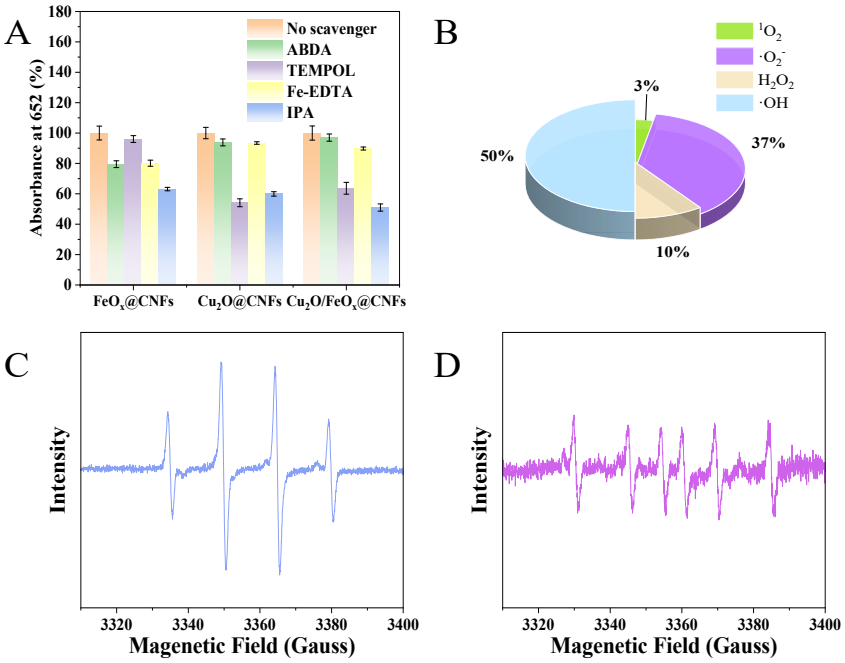

Figure S11. A) Absorbance at 652 nm of TMB reaction systems after adding different free radical quenching agents. B) Specific contributions of different ROS species in POD-like reaction. The ESR spectrum of C) ·OH and D) $O_2^{\cdot-}$.

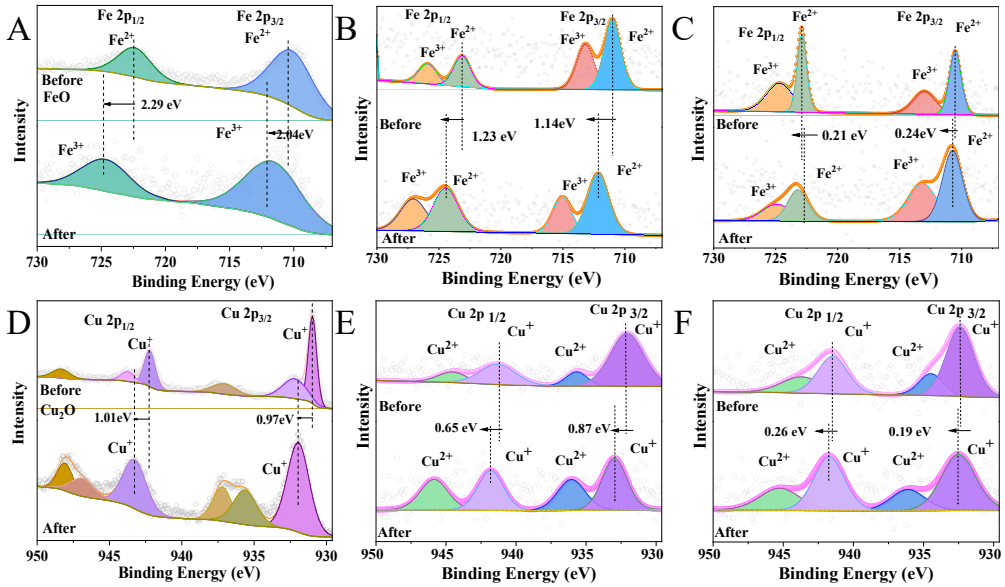

Figure S12. XPS spectra of Fe 2p in A) FeO, B) FeO_x@CNFs and C) Cu_2O/FeO_x@CNFs, and Cu 2p in D) Cu_2O, E) Cu_2O@CNFs and F) Cu_2O/FeO_x@CNFs before and after the POD-like reaction.

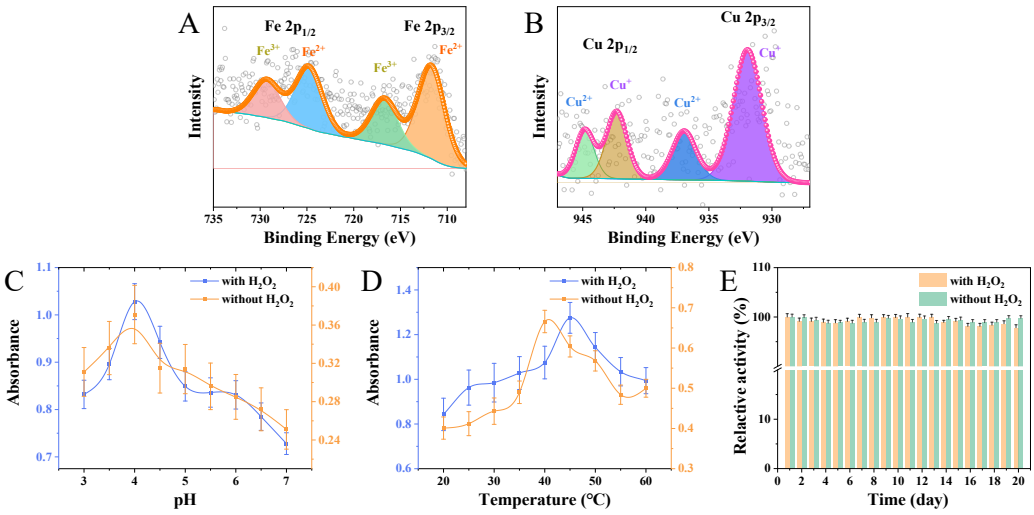

Figure S13. XPS spectra of A) Fe 2p and B) Cu 2p in Cu_2O/FeO_x@CNFs after 10 reaction cycles. Effect of C) pH and D) temperature on the enzyme-like activities. E) Long-term stability test of nanozymes on the enzyme-like activities.

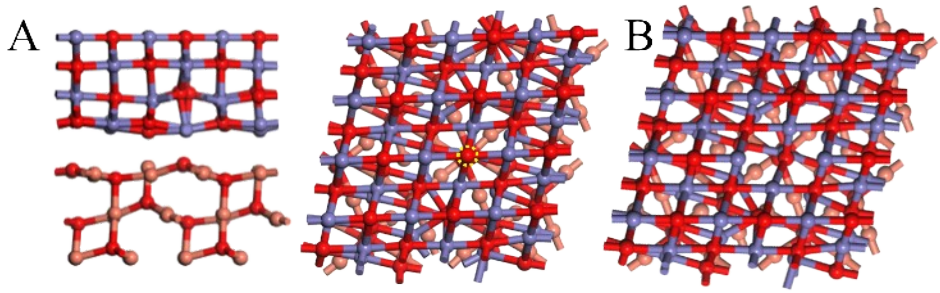

Figure S14. A) The optimized models of Cu_2O/FeO. B) The optimized models of Cu_2O/FeO_x with Ovs (the site of the Ovs is delineated with the yellow circle in the left figure).

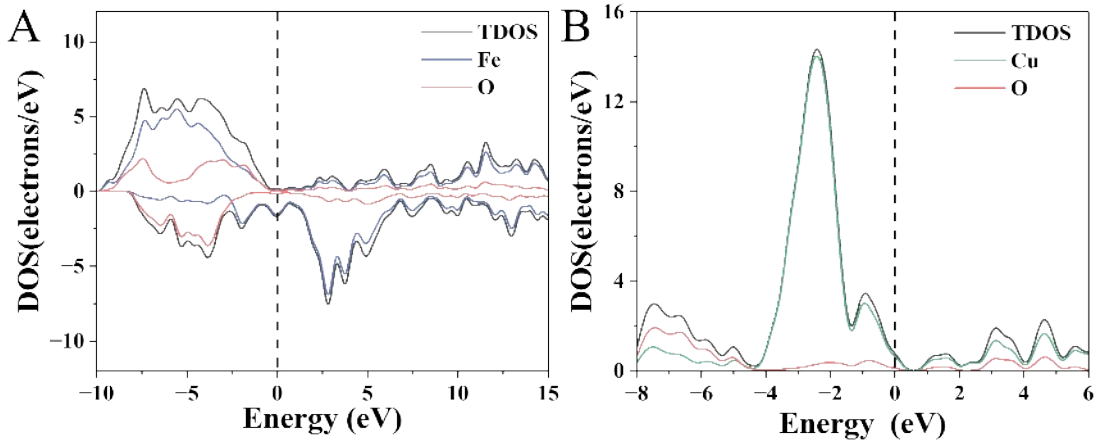

Figure S15. DOS of A) FeO and B) Cu_2O.

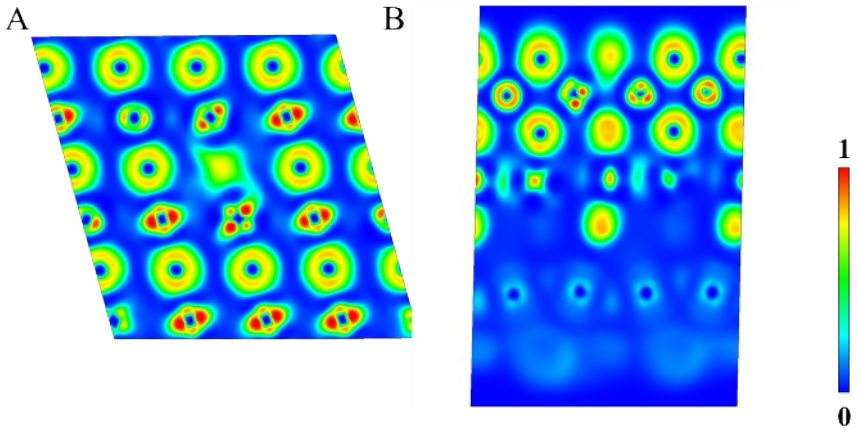

Figure S16. ELF two-dimensional slices of Cu_2O/FeO_x interface A) in the (0,0,1) direction, B) in the (0,1,0) direction.

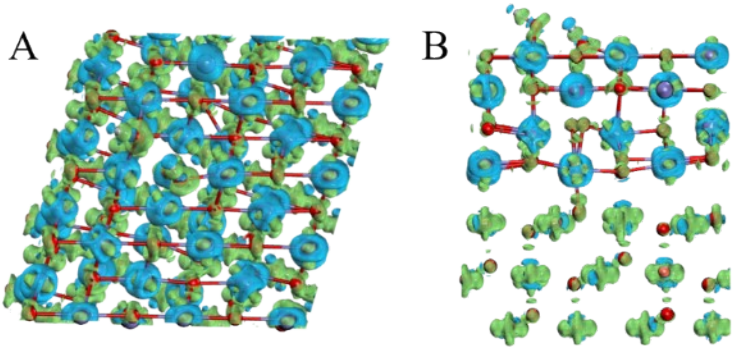

Figure S17. Electron density difference of Cu_2O/FeO_x-*2OH A) in the (0,0,1) direction and B) in the (0,1,0) direction. Green and blue regions represent electron accumulation and electron depletion, respectively.

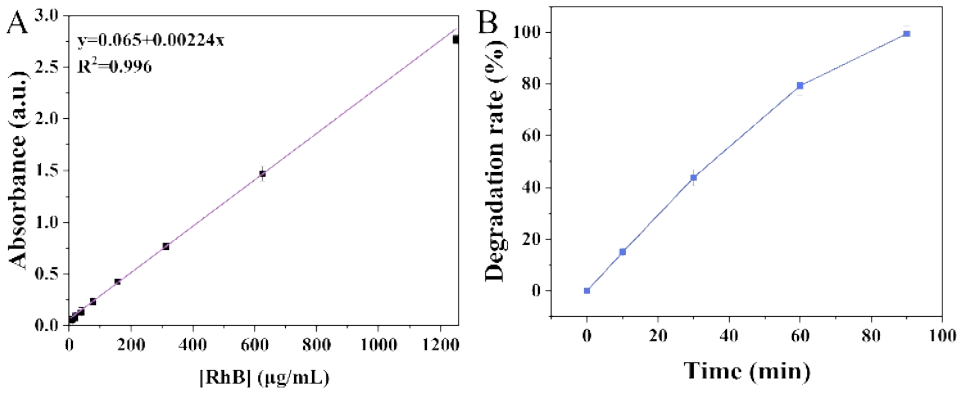

Figure S18. A) The corresponding calibration curves for RhB. B) The degradation rate of RhB treated with Cu_2O/FeO_x@CNFs + H_2O_2 at different times.

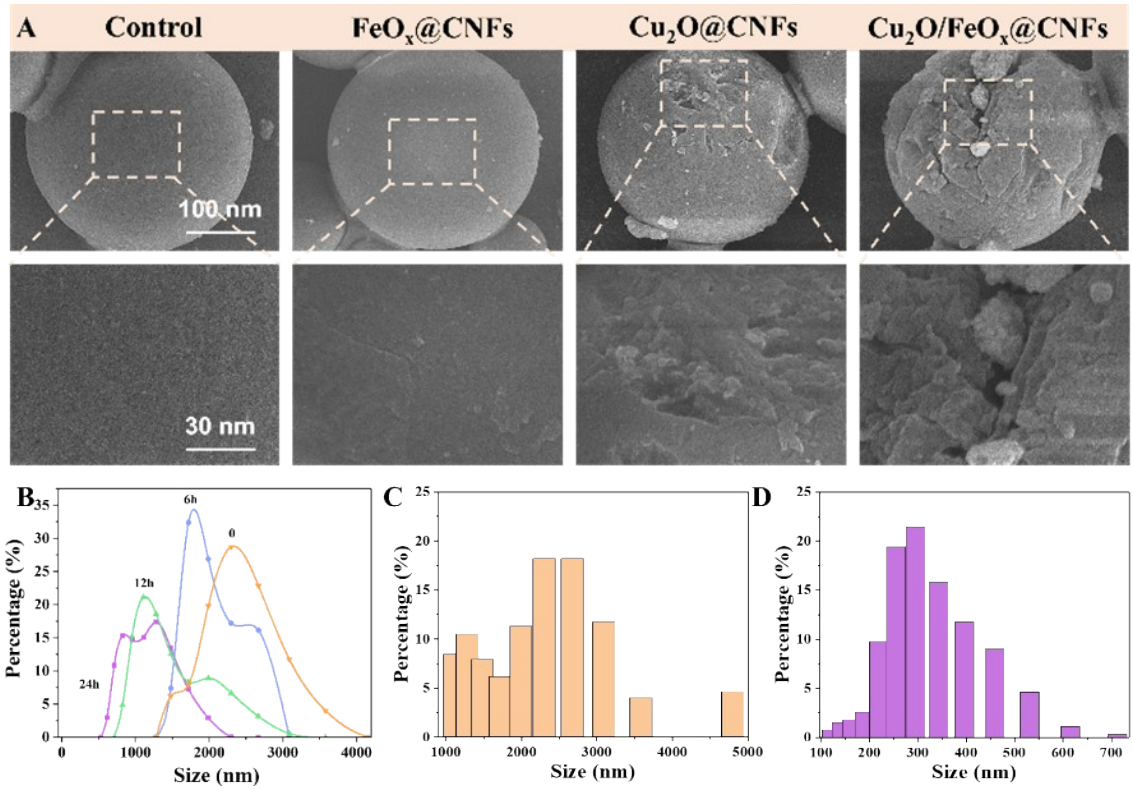

Figure S19. A) Higher-resolution SEM images of MPs treated by different materials + H_2O_2 for 24 hours. B) Particle size of MPs after Cu_2O/FeO_x@CNFs + H_2O_2 treatment at different times. Quantitative size distribution data of MPs C) before and D) after Cu_2O/FeO_x@CNFs + H_2O_2 treatment.

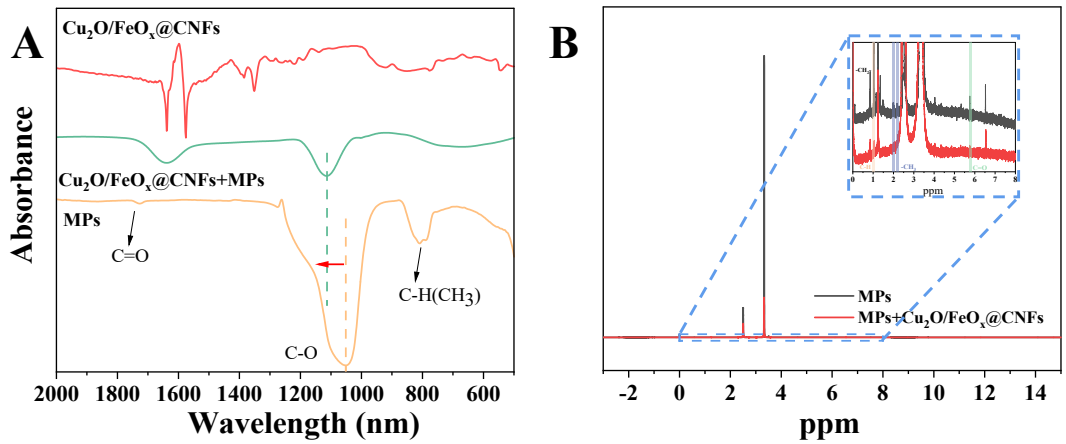

Figure S20. A) FTIR spectra of different materials. B) ^{1}H NMR spectra of different materials.

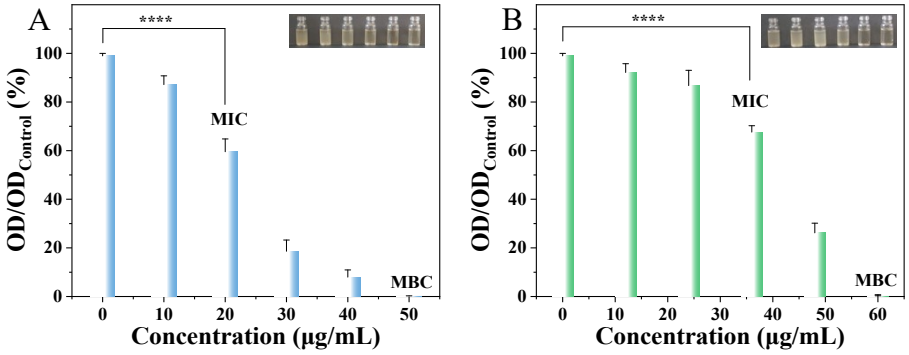

Figure S21. MIC and MBC of Cu_2O/FeO_x@CNFs + H_2O_2 antibacterial system against A) *E. coli* and B) *S. aureus*.

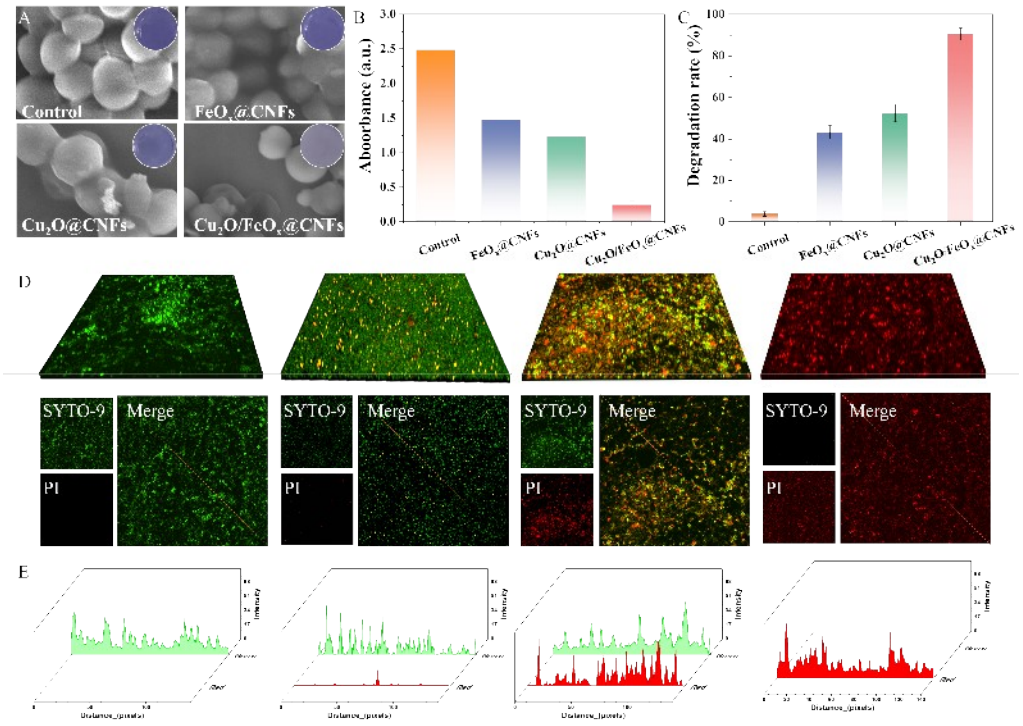

Figure S22. A) SEM images of *S. aureus* biofilms treated by H_2O_2 (Control), FeO_x@CNFs + H_2O_2, Cu_2O @CNFs + H_2O_2 and Cu_2O/FeO_x@CNFs + H_2O_2. Inset: pictures of crystal violet-stained *S. aureus* biofim. B) Absorbance at 509 nm of different reaction systems. C) Biofilm degradation rate of *S. aureus* under different treatments. D) 3D confocal laser scanning microscopy (CLSM) and fluorescence imaging of *S. aureus* dyed by SYTO-9 (dye for live bacteria)/PI (dye for dead bacteria). From left to right: bacteria treated by H_2O_2, FeO_x@CNFs + H_2O_2, Cu_2O@CNFs + H_2O_2 and Cu_2O/FeO_x@CNFs + H_2O_2. E) The linear distribution of colours along the dashed line in D, representing the density of live/ dead bacteria.

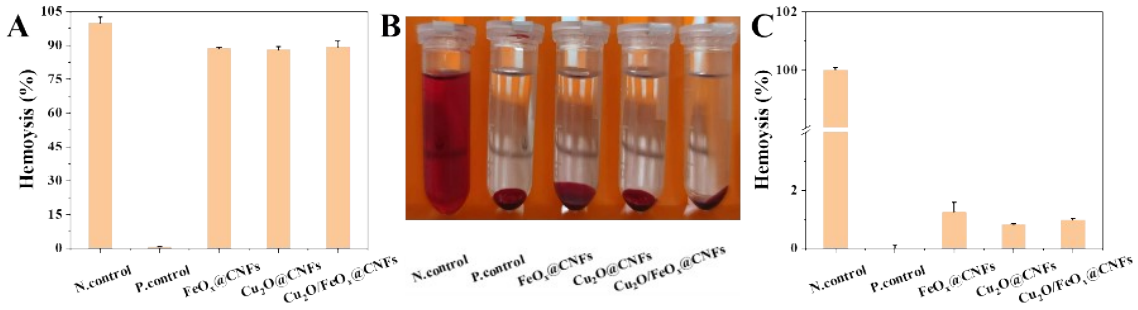

Figure S23. A) The cytotoxicity detection of 3T3-L1 by different material concentrations under treatment of each group. B) Hemolysis and C) hemolysis rate of erythrocytes in each group (N.control for negative control, P.control for positive control).

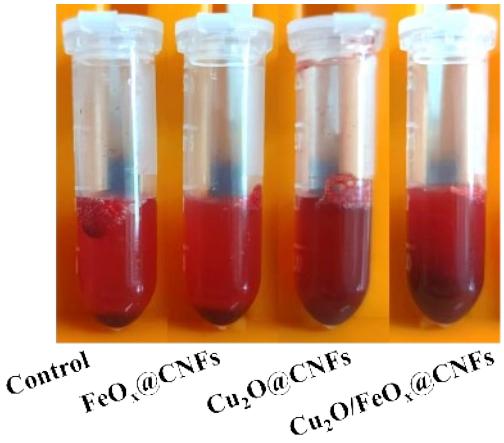

Figure S24. Whole blood-clotting test of each group.

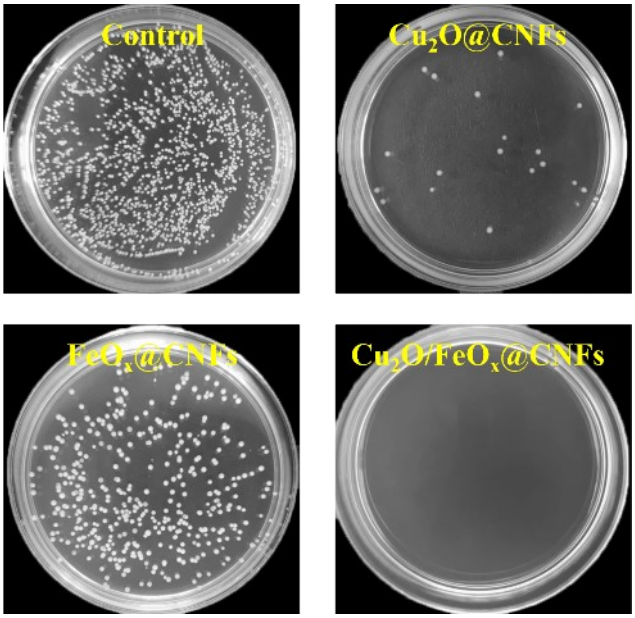

Figure S25. Survival bacteria clones on agar plates under different treatments.

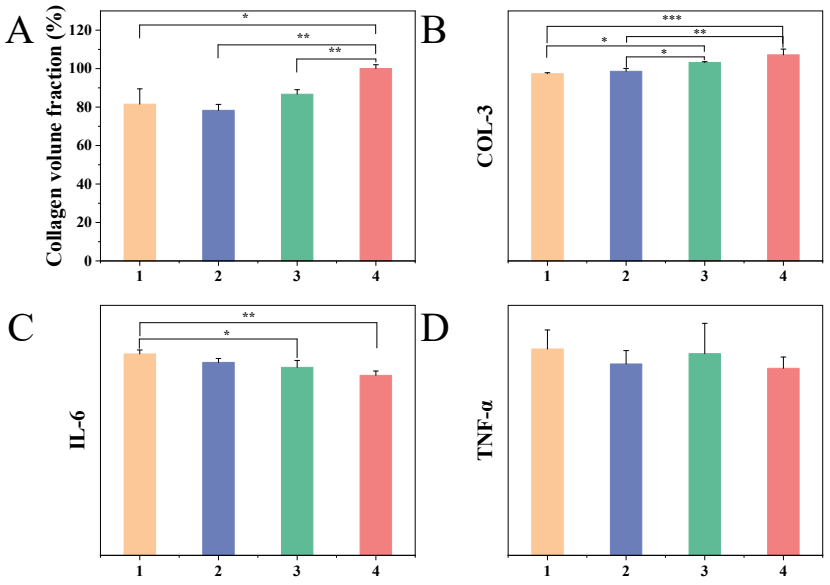

Figure S26. A) Statistical analysis of collagen deposition. B) The relative expression levels of B) COL-3, C) IL-6 and D) TNF-α of the wound area treated with 1: PBS, 2: FeO_x@CNFs + H_2O_2, 3: Cu_2O@CNFs + H_2O_2, 4: Cu_2O/FeO_x@CNFs + H_2O_2.

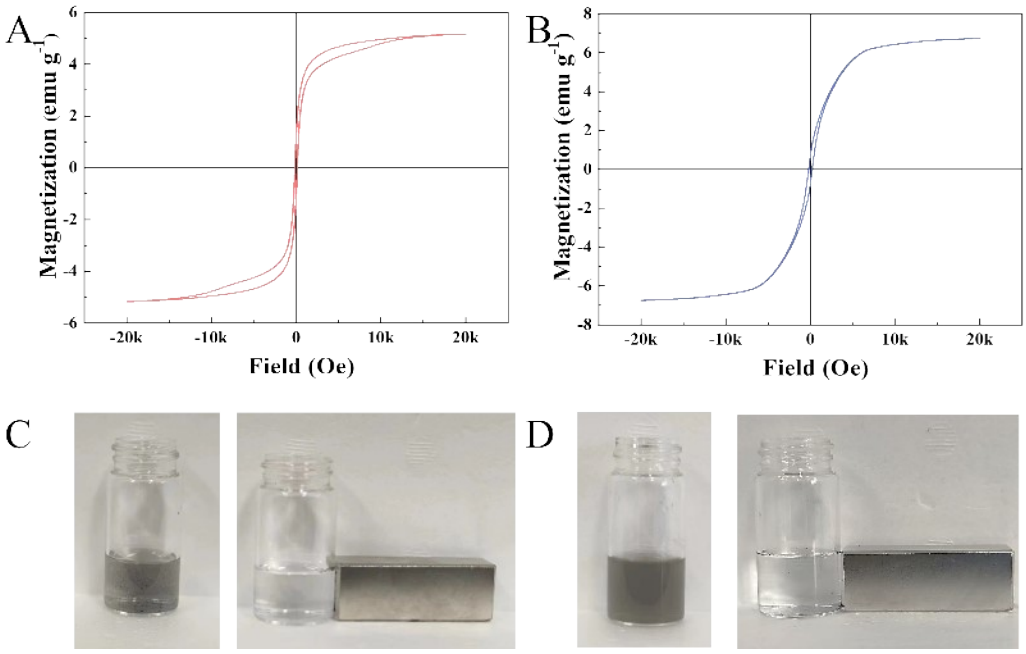

Figure S27. Vibrating sample magnetometer curves of the A) FeO_x@CNFs and B) Cu_2O/FeO_x@CNFs. Photographs depicting magnetic removal of C) FeO_x@CNFs and D) Cu_2O/FeO_x@CNFs.

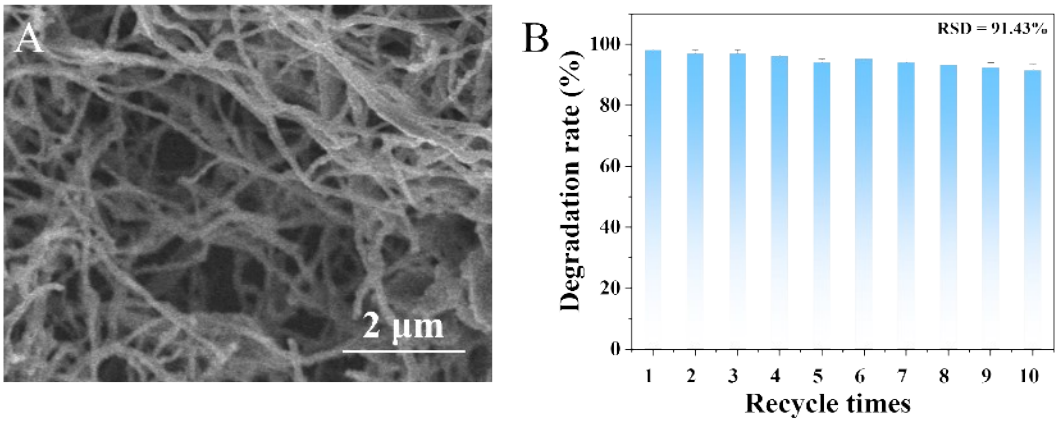

Figure S28. A) SEM image of recycled Cu_2O/FeO_x@CNFs. B) Recyclability of Cu_2O/FeO_x@CNFs.

Table S1. EXAFS fitting parameters at the Fe K-edge.

	Shell	CN	R(Å)	σ^2	ΔE_0	R factor
Cu_2O/FeO_x @CNFs	Fe-O	2.0±0.1	1.89±0.19	0.0180	1.3±2.1	0.0046
	Fe-Fe	4.0±0.3	2.44±0.01	0.0095		
	Fe-Cu	4.0±0.4	3.36±0.32	0.0142		

Table S2. EXAFS fitting parameters at the Cu K-edge.

	Shell	CN	R(Å)	σ^2	ΔE_0	R factor
Cu_2O/FeO_x @CNFs	Cu-O	2.0±0.1	1.98±0.14	0.0117	3.1±0.9	0.0152
	Cu-Cu	12.0±0.4	2.58±0.02	0.0123		
	Cu-Cu	12.0± 0.5	3.01±0.17	0.0112		

CN – coordination numbers,

R – bond distance,

σ^2– Debye-Waller factors,

ΔE_0– the inner potential correction.

R factor – goodness of fit.

Table S3. Comparison of the K_m and V_{max} values with other peroxidase mimetics.

Catalyst	K_m (mM)		V_{max} (10^{-8} M s^{-1})		Ref.
	H_2O_2	TMB	H_2O_2	TMB	
Cu_2O/FeO_x@CNFs	0.038	0.070	29.603	39.683	This work
HRP	3.700	0.434	8.710	10.000	(1)
MoS_2/g-C_3N_4HNs	0.15	1.32	13.02	7.27	(2)
MoS_2/g-C_3N_4	3.69	0.39	5.23	8.52	(2)
Fe_3O_4@MoS_2	1.390	0.250	16.310	11.100	(3)
Fe_3O_4@MoS_2-1%Ag	3.700	0.430	8.700	10.000	(3)
IN@AuNP	0.115	0.282	23.156	22.900	(4)
CuNPs/CoO/CNFs	0.26	0.14	12.32	42.24	(5)
Ru/CeO_2	0.053	2.68	26.01	3.03	(6)
CS@Fe/CDs	0.156	0.174	10.758	7.35	(7)
RuO_2/IrO_2	0.0636	0.0275	23.80	16.43	(8)

Table S4. MIC and MBC of Cu_2O/FeO_x@CNFs/H_2O_2 antibacterial system against different bacterial strains.

Bacterial strain	Gram bacteria classification	MIC (μg mL^{-1})	MBC (μg mL^{-1})
E. coli (ATCC25922)	Gram-positive	20	50
S. aureus (ATCC25923)	Gram-negative	36	60

References

1. Y. Tao, E. G. Ju, J. S. Ren and X. G. Qu, *Adv. Mater.*, 2015, 27, 1097–1104.
2. X. N. Liu, L. J. Huang, Y. P. Wang, J. Sun, T. L. Yue, W. T. Zhang and J. L. Wang, *Sens. Actuators, B*, 2020, 306.
3. F. Wei, X. Y. Cui, Z. Wang, C. C. Dong, J. D. Li and X. J. Han, *Chem. Eng. J.*, 2021, 408.
4. S. W. Zhao, D. Y. Wang, Q. Zhou, B. B. Wang, Z. Tong, H. L. Tian, J. K. Li and Y. H. Zhang, *Int. J. Biol. Macromol.*, 2024, 262.
5. P. B. Niu, Y. Q. Wang, R. Hu and T. Yang, *ACS Appl. Nano Mater.*, 2024, 7, 5996–6004.
6. Y. Chu, B. Cao, Y. S. Wang, X. X. Zhu, G. J. Li, Z. D. Yang and Q. Y. Liu, *Colloids Surf., A*, 2023, 679.
7. T. Pan, H. H. Chen, X. Gao, Z. Y. Wu, Y. W. Ye and Y. Z. Shen, *J. Hazard. Mater.*, 2022, 435.
8. D. Y. Wang, S. W. Zhao, J. K. Li, L. Shi, Y. H. Zhang, *Chem. Eng. J.* **2024,** *481*.